Available online at www.sciencedirect.com

ScienceDirect

Ceramics International 40 (2014) 4753–4757

CERAMICS INTERNATIONAL

www.elsevier.com/locate/ceramint

Non-lead Ce: $Na_{0.5}Bi_{0.5}TiO_3$–$BiFeO_3$ solid solution thin film with significantly reduced leakage current and large polarization

C.H. Yang[a,b,c,*], H.T. Wu[a,c], F. Yang[a], G.D. Hu[a]

[a]School of Materials Science and Engineering, University of Jinan, Jinan 250022, China
[b]State Key Laboratory of Crystal Materials, Shandong University, Jinan 250100, China
[c]Shandong Provincial Key Laboratory of Preparation and Measurement of Building Materials, University of Jinan, China

Received 20 August 2013; accepted 5 September 2013
Available online 12 September 2013

Abstract

The preferentially (100)-oriented $0.9Na_{0.5}Bi_{0.5}TiO_3$–$0.1BiFeO_3$ (NBT–BFO) solid solution thin films with and without Ce substitution were grown on a $LaNiO_3$(100)/Si substrate via a metal organic decomposition method. The effects of Ce doping on the crystalline structure, leakage current and ferroelectric property of NBT–BFO thin film were investigated. The diffraction peaks of NBT–BFO shift to higher diffraction angle as a result of shrinkage in the unit-cell volume by Ce substitution. At higher electric fields, the NBT–BFO film presents Poole–Frenkel emission consistent with the high leakage current, whereas in the Ce-doped NBT–BFO film, the dominant mechanism is changed to space-charge-limited conduction, and the leakage current density is reduced by two orders of magnitude. Compared with rounded ferroelectric polarization hysteresis loops of NBT–BFO film, substantial enhancement of ferroelectricity has been achieved in Ce-doped NBT–BFO film, with a remanent polarization (P_r) of 32.3 μC/cm^2. The capacitance–voltage curves of Ce-doped NBT–BFO film show butterfly shape, and the degree of ferroelectricity is enhanced more and more with increasing applied voltage.

Keywords: A. Films; B. Microstructure; B. X-ray methods; C. Electrical properties

1. Introduction

Recently, due to the increasing environmental problems, the high-performance lead-based piezoelectric compounds such as the $Pb(Zr,Ti)O_3$ family have been legally restricted in widely used integrated devices. Out of the various other possibilities, the A-site complex perovskite $Na_{0.5}Bi_{0.5}TiO_3$ has been considered as one of the key candidates [1,2]. Nonetheless, at present, the ferroelectric and piezoelectric properties of $Na_{0.5}Bi_{0.5}TiO_3$ cannot be compared with those of the lead-based family [3,4]. To improve the electrical performance, one approach is to dope $Na_{0.5}Bi_{0.5}TiO_3$ with an appropriate ferroelectric material to form a solid solution. $BiFeO_3$ is a well-known lead-free multiferroic material with a very large ferroelectric remanent polarization (P_r) of up to ~55 μC/cm^2 [5]. It is also a rhombohedral perovskite belonging to the R3c space group, which is the same as that of $Na_{0.5}Bi_{0.5}TiO_3$. Previous work has shown that $Na_{0.5}Bi_{0.5}TiO_3$ and $BiFeO_3$ can form a continuous R3c solid solution ceramic material at room temperature [6], and thus, $BiFeO_3$ is highly compatible for coupling with $Na_{0.5}Bi_{0.5}TiO_3$. Till now, little investigation has been carried out on $Na_{0.5}Bi_{0.5}TiO_3$ thin film with a small concentration of $BiFeO_3$ dopant.

The electrical characterization of a ferroelectric film is fundamentally based on three type of measurements: polarization–electric field hysteresis loop (P–E), current–voltage (I–V), and capacitance–voltage (C–V) characteristics. In this experiment, these measured results have been analyzed and correlated in the case of $Na_{0.5}Bi_{0.5}TiO_3$–$BiFeO_3$ films with and without Ce substitution. In addition, in order to minimize the additional effects caused by randomly-oriented polycrystalline films [7], (100)-oriented $Na_{0.5}Bi_{0.5}TiO_3$–$BiFeO_3$-based solid solution thin films were fabricated. In this work, Ce doping

*Corresponding author at: School of Materials Science and Engineering, University of Jinan, Jinan 250022, China. Tel.: +86 531 889736280; fax: +86 531 87974453.
E-mail address: mse_yangch@ujn.edu.cn (C.H. Yang).

0272-8842/$ - see front matter © 2013 Elsevier Ltd and Techna Group S.r.l. All rights reserved.
http://dx.doi.org/10.1016/j.ceramint.2013.09.019

of $Na_{0.5}Bi_{0.5}TiO_3$–$BiFeO_3$ thin film has been investigated as a means of improving the insulating and ferroelectric properties. Un-doped $Na_{0.5}Bi_{0.5}TiO_3$–$BiFeO_3$ thin film was also studied for comparison.

2. Experimental procedure

(100)-oriented un-doped $0.9Na_{0.5}Bi_{0.5}TiO_3$–$0.1BiFeO_3$ (NBT–BFO) and $0.9Na_{0.5}Bi_{0.5}TiO_3$–$0.1BiFeO_3$ + 0.5 mol% $Ce(NO_3)_3 \cdot 6H_2O$ (Ce: NBT–BFO) thin films were fabricated on a $LaNiO_3$ (LNO)(100)/Si substrate by metal organic decomposition. The details of the preparation of the precursor solutions have been reported elsewhere [8]. The precursor solution was deposited onto LNO(100)/Si by spin coating and annealed layer by layer at 500 °C for 10 min. Au top electrodes were deposited on the film using a sputtering system through a shadow mask with a diameter of 200 μm for electrical measurements. The thicknesses of the two films were all estimated to be 300 nm, as measured by a step profilometer. The structure was examined using an X-ray diffractometer (XRD, Bruker D8). A standard ferroelectric tester (Radiant Technologies) was used to measure the insulating and ferroelectric properties. The *C–V* characteristic was measured using an impedance analyser (HP4294A).

3. Results and discussions

Fig. 1 displays the X-ray diffraction patterns of NBT–BFO and Ce: NBT–BFO films deposited on LNO(100)/Si. One can see that both films show similar structure and highly-orientated growth, as evidenced by strong (100) and (200) diffraction peaks, without detectable secondary phase or diffraction peaks from other directions. It is worth mentioning that the annealing temperature in this experiment was as low as 500 °C, which can be ascribed to the uniformity of the precursor solution and the low nucleation temperature of $BiFeO_3$, as well as the seeding effect of perovskite-structured oxide electrode. Compared with $Na_{0.5}Bi_{0.5}TiO_3$, the diffraction peaks of NBT–BFO are shifted towards lower angles, suggesting that $BiFeO_3$ dissolves into the lattice structure of $Na_{0.5}Bi_{0.5}TiO_3$ [8]. The Ce substitution, however, can make the peaks of NBT–BFO shift slightly to higher diffraction angles due to the fact that the ionic radius of Ce is smaller than those of the replaced Bi and Na, indicating that lattice distortion of the NBT–BFO ferroelectric layer is induced by Ce doping.

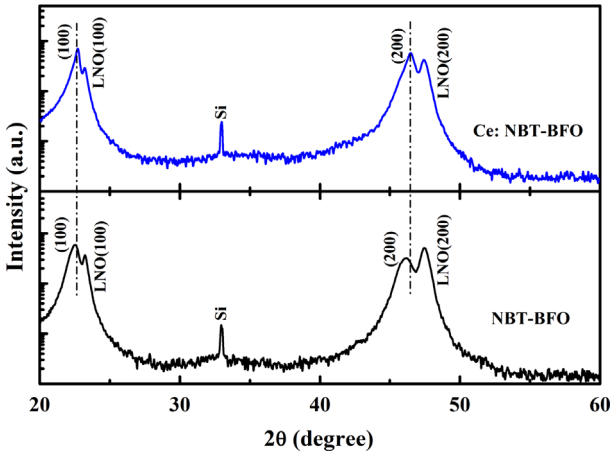

Fig. 1. XRD patterns for un-doped and Ce-doped NBT–BFO films fabricated on LNO(100)/Si annealed at 500 °C.

The current density versus electric field (*J–E*) characteristic of NBT, NBT–BFO and Ce: NBT–BFO films are shown in Fig. 2(a). As can be seen, the insulating property of NBT is improved slightly by BFO additive. However, the leakage current of NBT–BFO is reduced by about two orders of magnitude by Ce doping at higher electric field. The higher leakage current density of NBT and NBT–BFO can be ascribed to the extrinsic oxygen defects generated by the volatility of Bi or Na, and even the presence of Fe^{2+} and Fe'_{Ti}. In Ce: NBT–BFO, however, the Ce ions would occupy the A-site vacancies of V'''_{Bi} or V'_{Na}, resulting in a decreased total number of free carriers. Furthermore, the smaller grain sizes can be observed for Ce: NBT–BFO in AFM images (see Fig. 3). These factors can be responsible for the lower leakage current for Ce: NBT–BFO. To get further insight into the insulating properties, the conduction mechanisms for the NBT–BFO and Ce-doped specimens were investigated by fitting of the observed leakage current data, as shown in Fig. 2(b) and (c), respectively.

It can be seen that, for *E* higher than 170 kV/cm, the *J–E* curve of the NBT–BFO film is well fitted to the log–linear form $\log(J/E) \propto E^{1/2}$, as indicated by the solid line in Fig. 2(b). It is necessary to investigate whether the Poole–Frenkel (PF) emission dominates the *J–E* behavior for NBT–BFO. In PF emission, *J* can be determined by the following Equation [9,10]:

$$J_{PF} = BE\exp-\left(\frac{E_I}{kT} - \frac{q}{kT}\sqrt{\frac{qE}{\pi\varepsilon_0\varepsilon_r}}\right). \quad (1)$$

Therefore, the slope (α) of the $\log(J/E) - E^{1/2}$ curve (i.e., the optical-frequency ε_r) based on PF emission can be described as

$$\alpha = \frac{q^{3/2}}{kT\sqrt{\pi\varepsilon_0\varepsilon_r}}. \quad (2)$$

In Eqs. (1) and (2), *B* is a constant, *E* the applied electric field, E_I the ionization energy of the traps in the film, *k* the Boltzmann constant, *T* the absolute temperature, *q* the electronic charge, and ε_0 the permittivity of free space. The value of the relative optical-frequency permittivity, ε_r, calculated from the slope of the fitting is about 4 using Eq. (2). Moreover, the refractive index of pure $Na_{0.5}Bi_{0.5}TiO_3$ thin film has been reported to be $n = 2.16$ [11]. The optical-frequency permittivity can be then found to be $\varepsilon_r = n^2 = 4.67$ for $Na_{0.5}Bi_{0.5}TiO_3$, which is very close to the calculated ε_r value of the NBT–BFO film. Thus, we can conclude that the dominant conduction current at higher electric field in NBT–BFO film is dominated by PF emission. In the low field region, the fitting for NBT–BFO on a $\log(J/E) - E^{1/2}$ scale results in an unreasonable ε_r of 17, which excludes the PF conduction. A slope of about 1, however, is obtained in the log *J* versus log *E* plot, consistent with a contribution from Ohmic conduction ($J \propto E^{\alpha}$: $\alpha \approx 1$). Therefore, a combination of the two mechanisms is present for

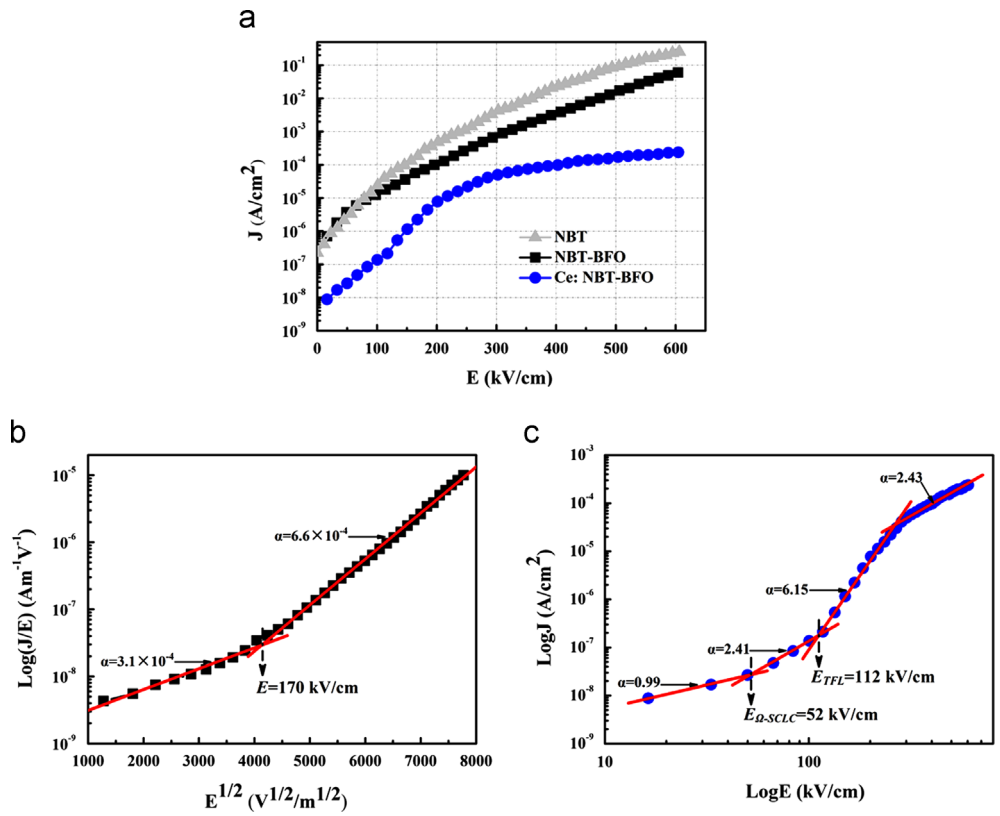

Fig. 2. (a) Leakage currents measured for NBT, NBT–BFO and Ce: NBT–BFO thin films, (b) plots of log(J/E) versus $E^{1/2}$ for NBT–BFO, and (c) log(J) versus log (E) for Ce: NBT–BFO.

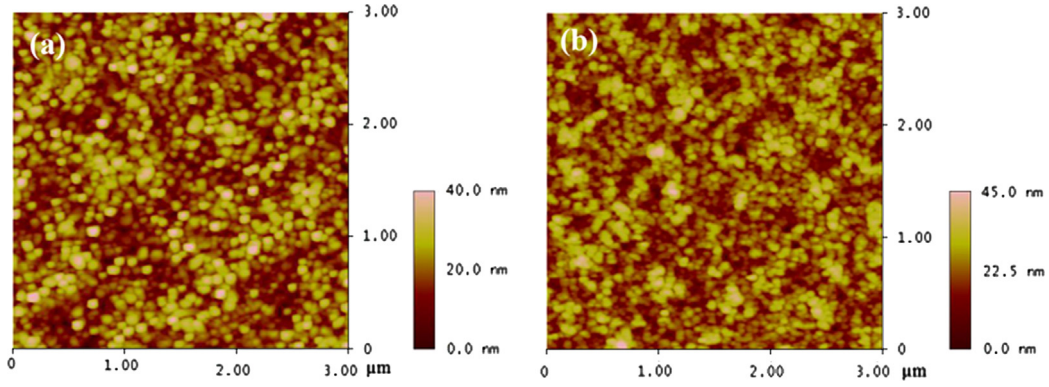

Fig. 3. AFM images of (a) NBT–BFO and (b) Ce: NBT–BFO thin films.

the NBT–BFO film. This is not surprising, as PF emission has normally been identified as the dominant mechanism in higher electric field in ferroelectric perovskite [10,12].

Fig. 2(c) exhibits a plot of log J versus log E for the Ce: NBT–BFO film. At low applied electric field, the curve follows normal Ohmic conduction ($J \propto E^{\alpha}$: $\alpha \approx 1$). In this region, the injected electrons from the electrode can be swiftly transported via the conduction band, resulting in a drift current. When the electric field increases, the curve can be modeled in terms of space-charge-limited current (SCLC). This type of conduction arises from the formation of space charge area, which acts to impede the current as charges are injected into the film from the electrode at a rate larger than that of travel though the film. The Ohmic to SCLC transition electric field, $E_{\Omega\text{-SCLC}}$, is given by Eq. (3) [13]. With increasing electric field, more electrons are injected into the film, and the empty traps are filled. The current density J increases exponentially at the rate of $\alpha = 2.41$, in the so-called trap-distributed region. Then, the current steeply rises with a slope of 6.15 on the double logarithmic plot because any further charge is then straightaway injected into the conduction band. The trap-filled voltage limit, E_{TFL}, can be expressed as Eq. (4) [13]. Finally, the slope becomes 2.43 according to Child's law conduction at high electric field. Therefore, there are also two types of

leakage current mechanisms, i.e., Ohmic and SCLC, competing to dominate as the electric field varies in the Ce: NBT–BFO film:

$$E_{\Omega-\mathrm{SCLC}} = \frac{8qn_0d}{9\theta\varepsilon_0\varepsilon_r}, \tag{3}$$

$$E_{\mathrm{TFL}} = \frac{8qdN_t}{9\varepsilon_0\varepsilon_r}. \tag{4}$$

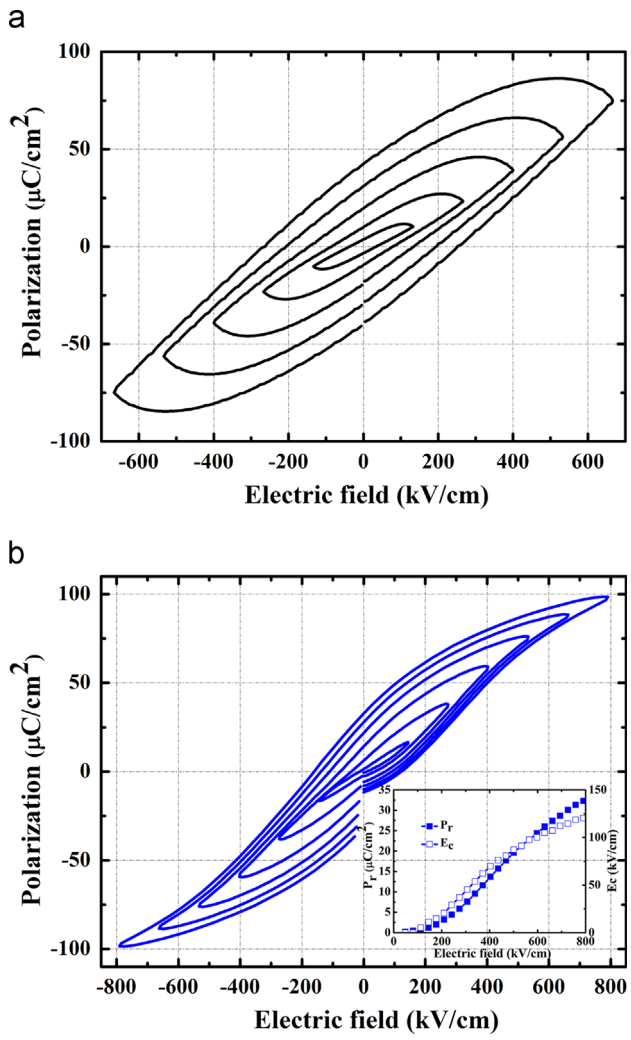

Fig. 4. Room temperature ferroelectric properties measured at 1 kHz in dynamic mode: (a) NBT–BFO film and (b) Ce: NBT–BFO film. The values of P_r and E_C of Ce: NBT–BFO as a function of the electric fields are shown in the inset.

In Eqs. (3) and (4), θ is a constant, n_0 the electron density of the film, ε_r the permittivity of film, ε_0 the permittivity of free space, q the electronic charge, d the thickness of the film, and N_t the concentration of shallow traps. Here, the $E_{\Omega\text{-SCLC}}$ and E_{TFL} for the NBT–BFO thin film can be estimated from the experimental results in Fig. 2(c) and are about 52 and 112 kV/cm, respectively.

Fig. 4 shows typical *P–E* hysteresis loops of the pure and Ce-doped NBT–BFO films. The *P–E* loops of NBT–BFO at different applied electric fields are all very round in shape. The "huge" polarization mainly originates from the charge injection and space charge contribution [14,15]. The leakage current in the NBT–BFO film was overwhelming, even after the applied voltage was reduced to 4 V. It can also be observed that the coercive field, E_C, is very high, which is also coupled with the low resistance. However, the NBT–BFO with Ce ion substitution shows much improved *P–E* loops, in which the electrical leakage feature is greatly reduced. At 800 kV/cm, the remnant polarization (P_r) is 32.3 μC/cm^2, which is among the highest in all the $Na_{0.5}Bi_{0.5}TiO_3$-based thin films reported so far [16–19]. Also, this value is much larger than that (~26 μC/cm^2) for $0.3Na_{0.5}Bi_{0.5}TiO_3$–$0.7Bi(Fe_{0.95}Mn_{0.05})O_3$ prepared by chemical solution deposition [20]. The coercive field ($E_C \approx 120$ kV/cm) for Ce: NBT–BFO is also about 50% smaller than that ($E_C \approx 250$ kV/cm) of the chemical solution deposition sample. It should be noted that the *P–E* loops for Ce: NBT–BFO are shifted along the electric field axis. This may be due to two factors: (i) the asymmetry of the top and bottom electrodes and (ii) the presence of internal bias. As can be seen from the inset of Fig. 3(b), the P_r and E_C of Ce: NBT–BFO tend to saturate as the applied electric field increases.

The normalized *C–V* curves were measured by sweeping the voltage from a negative bias to a positive one (up sweep) and then sweeping back (down sweep). In this measurement, hysteresis between the up- and down-sweep directions was observed, as shown in Fig. 5. Usually, the *C–V* curve exhibits a butterfly shape, in which the capacitance value measured at each bias voltage point represents the slope of the ferroelectric hysteresis (polarization–voltage: *P–V*) at the corresponding applied voltage. For Ce: NBT–BFO, the butterfly shape is obtained for all applied voltages. Higher capacitance variation (i.e., a relatively sharp feature), which is related to the polarization, is observed, especially at higher sweeping cut-off voltages higher than ± 16 V. This demonstrates that the degree of ferroelectricity of NBT–BFO is increased by doping with Ce ions [21]. The correlations between the *C–V*

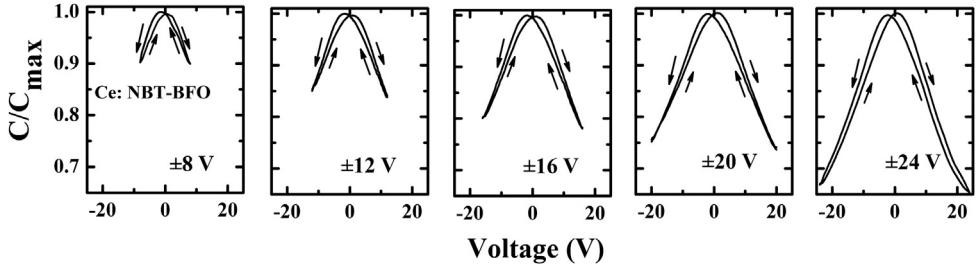

Fig. 5. The dc bias voltage dependence of the normalized capacitance for the Ce: NBT-BFO film.

characteristic and the *P–E* loop observed from Fig. 3(b) are indicated by two aspects: (i) the switching asymmetry observed in the *P–E* loop can also be found in the *C–V* curve and (ii) the applied voltages corresponding to the two maximum capacitances measured at certain sweeping voltages can be related to the corresponding coercive voltages (V_C). The V_C evaluated from the *C–V* measurement is usually smaller than that determined from the *P–E* loop, due to the fact that the *P–E* is acquired in a dynamic switching process, while the *C–V* is a quasistatic measurement [7].

4. Conclusions

In summary, preferential (100)-oriented Ce: NBT–BFO and NBT–BFO thin films have been successfully grown on an LNO(100)/Si substrate at the low temperature of 500 °C. Studies of leakage properties reveal that in higher electric fields, the dominating conduction mechanisms for NBT–BFO and Ce: NBT–BFO are PF emission and SCLC conduction, respectively. More importantly, Ce substitution can effectively suppress the leakage current of NBT–BFO, and thus induce a high remanent polarization P_r of 32.3 μC/cm^2. Futhermore, the *C–V* hysteresis curve is the fingerprint of the polarization reversal. Based on the above results, we can conclude that Ce-doped NBT–BFO solid solution thin films may have great potential for future applications in environment friendly ferroelectric devices.

Acknowledgments

This work was supported by the National Natural Science Foundation of China (No. 51002064) and the Open Research Project (No. KF1108) of the State Key Laboratory of Crystal Materials (Shandong University).

References

[1] H. Zhou, G.H. Wu, N. Qin, D.H. Bao, Improved electrical properties and strong red emission of Pr^{3+}-doped $xK_{0.5}Bi_{0.5}TiO_3$–$(1-x)Na_{0.5}Bi_{0.5}TiO_3$ lead-free ferroelectric thin films, Journal of the American Ceramic Society 95 (2012) 483–486.

[2] P. Rachakom, S. Jaiban, A. Jiansirisomboon,, Watcharapasorn, Crystal structure and electrical properties of bismuth sodium titanate zirconate ceramics, Nanoscale Research Letters 7 (2012) 57–61.

[3] D. Maurya, A. Pramanick, K. An, S. Priya, Enhanced piezoelectricity and nature of electrical-field induced structural phase transformation in textured lead-free piezoelectric $Na_{0.5}Bi_{0.5}TiO_3$–$BaTiO_3$ ceramics, Applied Physics Letters 100 (2012) 172906.

[4] H. Adachi, Y. Tanaka, T. Harigai, M. Ueda, E. Fujii, Large transverse piezoelectricity in strained (Na,Bi)TiO_3–$BaTiO_3$ epitaxial thin films on MgO(110), Applied Physics Express 4 (2011) 051501.

[5] J. Wang, J.B. Neaton, H. Zheng, V. Nagarajan, S.B. Ogale, B. Liu, D. Viehland, V. Vaithyanathan, D.G. Schlom, U.V. Waghmare, N. A. Spaldin, K.M. Rabe, M. Wuttig, R. Ramesh, Epitaxial $BiFeO_3$ multiferroic thin film heterostructures, Science 299 (2003) 1719–1722.

[6] V. Dorcet, P. Marchet, G. Trolliard, Structural and dielectric studies of the $Na_{0.5}Bi_{0.5}TiO_3$–$BiFeO_3$ system, Journal of the European Ceramic Society 27 (2007) 4371–4374.

[7] L. Pintilie, M. Lisca, M. Alexe, Polarization reversal and capacitance–voltage characteristic of epitaxial Pb(Zr,Ti)O_3 layers, Applied Physics Letters 86 (2005) 192902.

[8] C.H. Yang, G.D. Hu, W.B. Wu, H.T. Wu, F. Yang, L. Wang, Reduced leakage current, enhanced ferroelectric and dielectric properties in (Ce, Fe)-codoped $Na_{0.5}Bi_{0.5}TiO_3$ film, Applied Physics Letters 100 (2012) 022909.

[9] J. Frenkel, On the theory of electrical breakdown of dielectrics and electronic semiconductors, Technical Physics of the USSR 5 (1938) 685–687.

[10] Y. Shuai, S.Q. Zhou, S. Streit, H. Reuther, D. Bürger, S. Slesazeck, T. Mikolajick, M. Helm, H. Schmidt, Reduced leakage current in $BiFeO_3$ thin films with rectifying contacts, Applied Physics Letters 98 (2011) 232901.

[11] C.Y. Kim, T. Sekino, K. Niihara, Optical, mechanical, and dielectric properties of $Bi_{1/2}Na_{1/2}TiO_3$ thin film synthesized by sol–gel method, Journal of Sol–Gel Science and Technology 55 (2010) 306–310.

[12] G.W. Pabst, L.W. Martin, Y.-H. Chu, R. Ramesh, Leakage mechanisms in $BiFeO_3$ thin films, Applied Physics Letters 90 (2007) 072902.

[13] S.Y. Wang, B.L. Cheng, C. Wang, S.A.T. Redfern, S.Y. Dai, K.J. Jin, H. B. Lu, Y.L. Zhou, Z.H. Chen, G.Z. Yang, Influence of Ce doping on leakage current in $Ba_{0.5}Sr_{0.5}TiO_3$ films, Journal of Physics D: Applied Physics 38 (2005) 2253–2257.

[14] S. Lahmar, C.-H. Habouti, M. Solterbeck, M. Dietze, Es-Souni, Multiferroic properties of $Bi_{0.9}Gd_{0.1}Fe_{0.9}Mn_{0.1}O_3$ thin film, Journal of Applied Physics 107 (2010) 024104.

[15] Z.X. Cheng, X.L. Wang, S.X. Dou, Improved ferroelectric properties in multiferroic $BiFeO_3$ thin films through La and Nb codoping, Physical Review B 77 (2008) 092101.

[16] Q.G. Chi, F.Y. Yang, C.H. Zhang, C.T. Chen, H.F. Zhu, X. Wang, Q. Q. Lei, Influence of seed layer on crystal orientation and electrical properties of $(Na_{0.85}K_{0.15})_{0.5}Bi_{0.5}TiO_3$ thin films prepared by a sol–gel process, Ceramics International (2013).

[17] Y.Y. Wu, X.H. Wang, C.F. Zhong, L.T. Li, Effect of Mn doping on microstructure and electrical properties of the $(Na_{0.85}K_{0.15})_{0.5}Bi_{0.5}TiO_3$ thin films prepared by sol–gel method, Journal of the American Ceramic Society 94 (2011) 3877–3882.

[18] X.L. Fang, B. Shen, J.W. Zhai, X. Yao, Preparation and ferroelectric properties of $(Na_{0.5}Bi_{0.5})_{0.94}Ba_{0.06}TiO_3$ thin films deposited on Pt electrodes using $LaNiO_3$ as buffer layer, Ceramics International 38S (2012) S83–S86.

[19] M.M. Hejazi, E. Taghaddos, A. Safari, Reduced leakage current and enhanced ferroelectric properties in Mn-doped $Bi_{0.5}Na_{0.5}TiO_3$-based thin films, Journal of Materials Science 48 (2013) 3511–3516.

[20] A. Hieno, W. Sakamoto, M. Moriya, T. Yogo, Synthesis of $BiFeO_3$–$Bi_{0.5}Na_{0.5}TiO_3$ thin films by chemical solution deposition and their properties, Japanese Journal of Applied Physics 50 (2011) 09NB04.

[21] N.M. Murari, R. Thomas, R.E. Melgarejo, S.P. Pavunny, R.S. Katiyar, Structural, electrical, and magnetic properties of chemical solution deposited $BiFe_{1-x}Ti_xO_3$ and $BiFe_{0.9}Ti_{0.05}Co_{0.05}O_3$ thin films, Journal of Applied Physics 106 (2009) 014103.